Available online at www.sciencedirect.com

SciVerse ScienceDirect

Procedia IUTAM 7 (2013) 21 – 28

Procedia IUTAM

www.elsevier.com/locate/procedia

Topological Fluid Dynamics: Theory and Applications

Impulse of vortex knots from diagram projections

Renzo L. Ricca*

Department of Mathematics and Applications, University of Milano-Bicocca, Via Cozzi 53, 20125 Milano, Italy

Abstract

In this paper I extend the area interpretation of linear and angular momenta of ideal vortex filaments to complex tangles of filaments in space. A method based on the extraction of area information from diagram projections is presented to evaluate the impulse of vortex knots and links. The method relies on the estimate of the signed areas of sub-regions of the graph resulting from the projection of the vortex axes on the plane of the graph. Some examples based on vortex rings interaction, vortex knots and links are considered for illustration. This method provides a complementary tool to estimate dynamical properties of complex fluid flows and it can be easily implemented in real-time diagnostics to investigate fluid dynamical properties of complex vortex flows.

Selection and/or peer-review under responsibility of the Isaac Newton Institute for Mathematical Sciences, University of Cambridge

Keywords: Euler equations; linear momentum; angular momentum; vortex impulse; diagram analysis; vortex knots and links; topological fluid dynamics, structural complexity.

1. Area interpretation of linear and angular momenta under Euler equations

In this paper we show that linear and angular momenta of vortex filaments forming a complex network of curves in space can be computed in terms of signed area of projected diagrams. The area interpretation of momenta, first noticed by Lord Kelvin in 1875 [1] and proved by Arms & Hama [2, 3] in the context of LIA for filaments omeomorphic to the circle, seems to have received very little attention. What I present here is a straightforward extension of the area interpretation of momenta to complex graphs of nodal curves. The method presented here has great potential for further developments and future applications in diagnostics of complex fluid flows.

Let us first consider a single vortex filament $\mathcal{K}$ in an unbounded, ideal fluid at rest at infinity, where vorticity is confined to the filament. Such type of vortex arises naturally in superfluid turbulence [4, 5], where indeed vorticity remains localized for very long time on extremely thin filaments, with typical length of the order of 1 cm and vortex cross-section of the order of 10^{-8} cm.

Let $\mathcal{K} = \mathcal{K}(\chi)$ be centered on the filament axis χ, a smooth, simple, closed curve, possibly knotted, in $\mathbb{R}^3$, given by the position vector $\mathbf{X} = \mathbf{X}(s)$, where $s \in [0, L]$ is arc-length and L is total length. Let us assume that vorticity is simply given by $\boldsymbol{\omega} = \omega_0 \hat{\mathbf{t}}$, where ω_0 is constant and $\hat{\mathbf{t}} = \mathrm{d}\mathbf{X}/\mathrm{d}s$ is the unit tangent to χ, with orientation inherited by

* *E-mail address:* renzo.ricca@unimib.it

2210-9838
Selection and/or peer-review under responsibility of the Isaac Newton Institute for Mathematical Sciences, University of Cambridge
doi:10.1016/j.piutam.2013.03.004

the vorticity. The vortex circulation (quantized in the superfluid case), is given by

$$\Gamma = \oint_{\Sigma} \boldsymbol{\omega}\, \mathrm{d}^2\mathbf{X} = \text{constant}\ , \tag{1}$$

where Σ is the area of the vortex cross-section. The linear momentumt (per unit density) $\mathbf{P} = \mathbf{P}(\mathcal{K})$ corresponds to the hydrodynamic impulse, which generates the motion of $\mathcal{K}$ from rest; from standard definition [3] it takes the form

$$\mathbf{P} = \frac{1}{2}\int_V \mathbf{X}\times\boldsymbol{\omega}\, \mathrm{d}^3\mathbf{X} = \frac{1}{2}\Gamma\oint_{\mathrm{L}(\chi)} \mathbf{X}\times\hat{\mathbf{t}}\, \mathrm{ds} = \text{constant}\ , \tag{2}$$

where V is the filament volume. Similarly, for the angular momentum (per unit density) $\mathbf{M} = \mathbf{M}(\mathcal{K})$ (the moment of the impulsive forces acting on $\mathcal{K}$), given by

$$\mathbf{M} = \frac{1}{3}\int_V \mathbf{X}\times(\mathbf{X}\times\boldsymbol{\omega})\, \mathrm{d}^3\mathbf{X} = \frac{1}{3}\Gamma\oint_{\mathrm{L}(\chi)} \mathbf{X}\times(\mathbf{X}\times\hat{\mathbf{t}})\, \mathrm{ds} = \text{constant}\ . \tag{3}$$

Now evidently, since $\hat{\mathbf{t}}\, \mathrm{ds} = \mathrm{d}\mathbf{X}$, we have (see, for instance, [3], Sec. 11.1)

$$\oint_{L(\chi)} \mathbf{X}\times \mathrm{d}\mathbf{X} = 2\int_{\mathrm{A}} \mathrm{d}\hat{\mathbf{S}}\ , \quad \oint_{\mathrm{L}(\chi)} \mathbf{X}\times(\mathbf{X}\times\hat{\mathbf{t}})\, \mathrm{ds} = 2\int_{\mathrm{A}} \mathbf{X}\times\mathrm{d}\hat{\mathbf{S}}\ , \tag{4}$$

where $\hat{\mathbf{S}}$ denotes the oriented region bounded by $L(\chi)$ of unit normal $\hat{\boldsymbol{\nu}}$ and area A. Since both $\mathbf{P}$ and $\mathbf{M}$ are vector quantities, each vector component can be related to the *signed area* of the diagram resulting from the projection of χ along the direction of projection given by that component. In general, if we denote by $\Lambda = p(\chi)$ the planar curve projected along p, then Λ is a graph given by a nodal curve with self-intersections. In the case of a simple, non-self-interesecting, planar curve Λ, the area bounded by Λ is given by the standard geometric area A. If, however, Λ is given by a self-intersecting curve we have to consider the question of determining the area $\mathcal{A} = \mathcal{A}(\Lambda)$ of the planar graph bounded by Λ. This question will be addressed in the next section. In any case, we must have

$$p(\chi):\ \mathbb{R}^3 \to \mathbb{R}^2\ , \qquad \begin{cases} p_x : \Lambda_{yz}\ ,\ \mathcal{A}_{yz} = \mathcal{A}(\Lambda_{yz})\ , \\ p_y : \Lambda_{zx}\ ,\ \mathcal{A}_{zx} = \mathcal{A}(\Lambda_{zx})\ , \\ p_z : \Lambda_{xy}\ ,\ \mathcal{A}_{xy} = \mathcal{A}(\Lambda_{xy})\ . \end{cases} \tag{5}$$

Hence, by combining (2) and (3) with (4), we can write

$$\mathbf{P} = (P_x, P_y, P_z) = \Gamma(\mathcal{A}_{yz}, \mathcal{A}_{zx}, \mathcal{A}_{xy})\ , \tag{6}$$

$$\mathbf{M} = (M_x, M_y, M_z) = \frac{2}{3}\Gamma(d_x\mathcal{A}_{yz}, d_y\mathcal{A}_{zx}, d_z\mathcal{A}_{xy})\ , \tag{7}$$

where $d_x\mathcal{A}_{yz}$, $d_y\mathcal{A}_{zx}$, $d_z\mathcal{A}_{xy}$ are the areal moments according to the following definition (see, for instance, [1], Sec. 27).

Definition. The *areal moment* around any axis is the product of the area $\mathcal{A}$ multiplied by the distance d between that axis and the axis $\mathbf{a}_G$, normal to $\mathcal{A}$ through the centroid G of $\mathcal{A}$.

Hence, d_x, d_y, d_z denote the Euclidean distances of the area centroid G from the axes x, y, z, respectively. In the following section we shall address the question of computing the area $\mathcal{A}$ of a complex graph.

2. Signed area of a planar graph

Let us consider now a planar graph Λ resulting from a projection of a space curve χ onto $\mathbb{R}^2$. A graph diagram is a *good projection*, when it has at most double points, i.e. nodal points given by at most two intersecting arcs. Note that it is always possible to reduce highly complex graph diagrams to good nodal curves [6]. In general we consider graphs made by a finite number of sub-regions R_j (see Figure 1a). Since χ is oriented, Λ inherits the orientation by the projection p. If Λ is simple, the bounded region will be unambiguously oriented by Λ. For a complex graph,

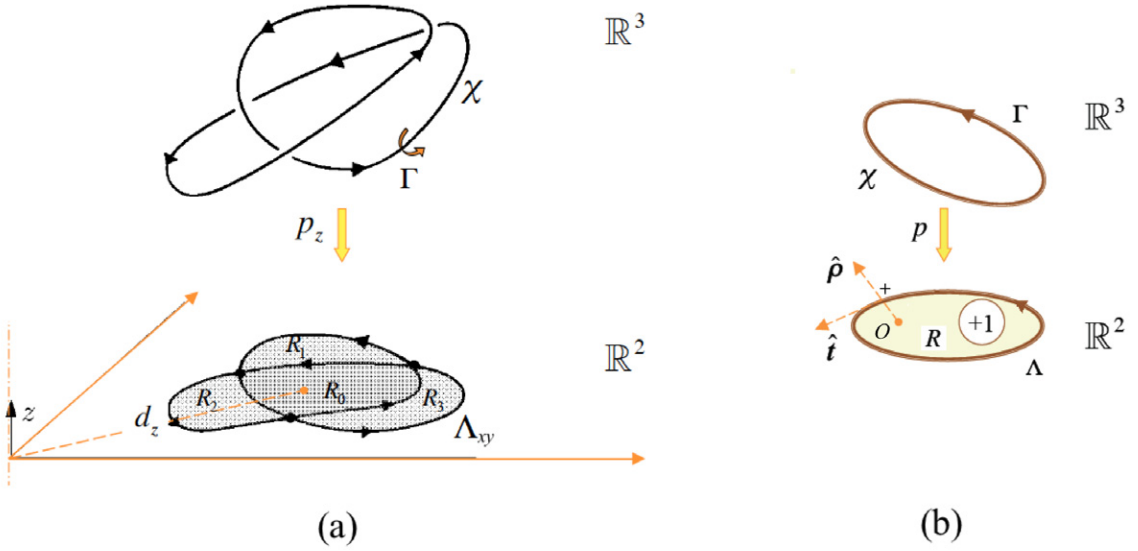

Fig. 1. The projection p of a space curve χ (centerline of a vortex filament of circulation Γ) is likely to generate a nodal curve (a graph) Λ, that bounds the plane in sub-regions R_j. (a) The graph Λ_{xy}, shown in the figure, bounds 4 sub-regions, $R_0, \ldots, R_3$. Note that the orientation of the bounding arcs of each sub-region is not necessarily congruent. (b) The signed area of R is given by the standard area of R multiplied by the index $\mathcal{I}$, that in this case is $+1$.

however, each sub-region R_j may be bounded by oriented arcs, whose relative orientations may *not* be necessarily congruent (see, for example, R_1, R_2 and R_3 of Figure 1a). Apparently it was C.F. Gauss [7], who first addressed in a letter to H. Olbers the question of determining the area "content" (*Inhalt*) of a planar graph. To determine this, let us choose a radial vector line along $\hat{\boldsymbol{\rho}}$, with arbitrary footpoint O in R and arbitrary direction outwardly (see Figure 1b), and the positive reference given by the pair of unit vectors $(\hat{\boldsymbol{\rho}}, \hat{\mathbf{t}})$. For any given direction $\hat{\boldsymbol{\rho}}$, let us consider the points of intersection given by the $\hat{\boldsymbol{\rho}}$-line as it crosses successively the bounding arcs of the plane graph. For the simple case shown in Figure 1b, where there is only one bounding curve, there will be only one intersection point, but in general an internal region R_j of Λ will be surrounded by the arcs forming the graph. To each intersection point let us assign the value $\epsilon = \pm 1$, according to the reference $(\hat{\boldsymbol{\rho}}, \hat{\mathbf{t}})$ associated with each oriented arc.

Definition. The *index* $\mathcal{I}_j$ of the region R_j of $\Lambda \in \mathbb{R}^2$, is given by

$$\mathcal{I}_j = \sum_{r \in \{\hat{\boldsymbol{\rho}} \cap \Lambda\}} \epsilon_r \ , \tag{8}$$

where $\{\hat{\boldsymbol{\rho}} \cap \Lambda\}$ denotes the set of intersection points given by the $\hat{\boldsymbol{\rho}}$ vector with the arcs of the graph Λ, and $\epsilon_r = \pm 1$, according to the reference $(\hat{\boldsymbol{\rho}}, \hat{\mathbf{t}})$ at each intersection point of Λ.

The index above is reminiscent of the Cauchy index of real rational functions. It can be easily proved that the index $\mathcal{I}_j$ depends only on the region R_j and is independent of the choice of the position of the footpoints O_j and of the direction of the $\hat{\boldsymbol{\rho}}_j$-lines. Indeed this can be interpreted as the linking coefficient in $S^2 = \mathbb{R}^2 \cup \{\infty\}$ of the 0-cycle $(\infty - O_j)$ and the 1-cycle Λ (Claude Weber, private communication). We can now define the signed area of a graph region according to the following:

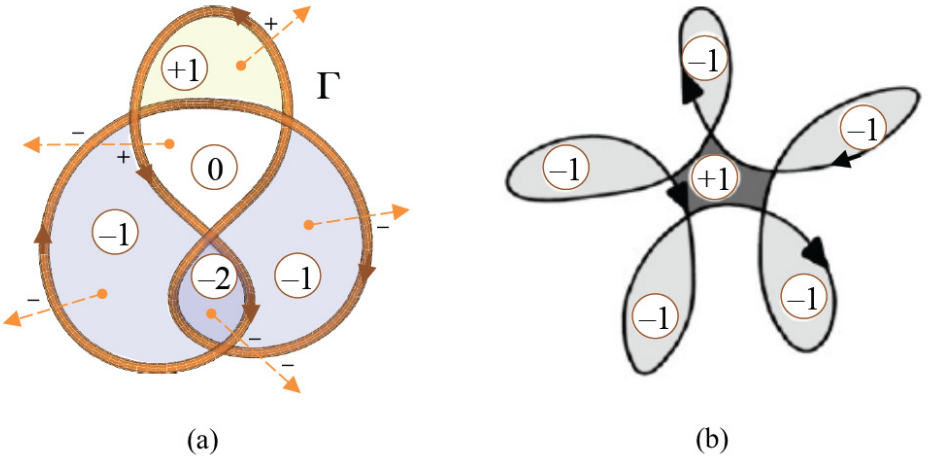

Fig. 2. (a) The figure-of-eight knot shown in an "indented" projection (by allowing small indentations in the projection plane to make visible under-crossings and over-crossings). In a standard plane projection all crossings collapse to nodal points. Note the contributions from the crossing signs to the index computation of each region. (b) A poloidal coil in a standard plane projection. The encircled values denote the indices $\mathcal{I}_j$ associated with their respective regions.

Definition. The *signed area* of a region R_j is given by

$$\mathcal{A}_j(R_j) = \sum_j \mathcal{I}_j A_j(R_j) \,, \tag{9}$$

where $A_j(R_j)$ denotes the standard area of R_j.

The signed area extends the concept of standard area for regions determined by graphs of nodal curves and, by elementary homology (interpreting Λ as a 1-cycle and the graph regions as a 2-chain), it can be proven to provide the effective correct computation of the area of a graph. It is this signed area that will be used in the computation of the momenta.

Note that the sign convention is consistent with the expected sign of the impulse of a vortex ring. Since vortex filament motion is (to first approximation) dominated by curvature effects along the binormal direction, the algebraic sign of the index $\mathcal{I}$ must be in agreement with the contribution given by the bounding arcs to the momentum of the system (see Figure 1b).

3. Examples of computation of signed areas for complex graphs

3.1. Single-component systems: knots

Figure-of-eight knot. Let us consider the diagram of Figure 2a and evaluate the indices $\mathcal{I}_j$. Suppose that this diagram results from the projection of a figure-of-eight knot (in the diagram shown we kept track of over-crossings and under-crossings for visualization purposes only; in the standard, planar projection all the crossings become nodal points, and we loose track of any topological information). For each region we choose (arbitrarily) a radial vector and for each vector we consider the intersections of the $\hat{\boldsymbol{\rho}}$-line with the graph. At each intersection we assign a $+1$ or a -1, according to the positive reference defined in the previous section, and we sum up all the contributions according to (8), hence determining the index of that region. Their values are shown encircled in Figure 2a. These values are topological in character, because they do not depend on the choice of the footpoint of $\hat{\boldsymbol{\rho}}$, providing a multiplying factor

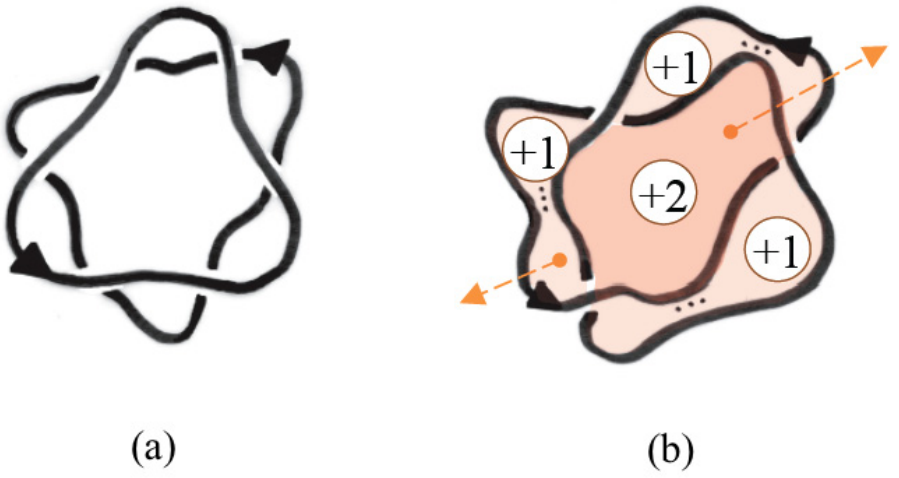

Fig. 3. (a) Two vortex ring interact and (b) reconnect to form a trefoil knot. The central region, having largest area and highest index, is likely to move more rapidly than the rest of the system in the normal direction to the projection plane.

for the standard area. For instance, by using eq. (5) we see that the central region of the figure-of-eight knot with index 0 will not contribute to the impetus in the direction normal to this plane projection, whereas the nearby regions, with relative indices $+1$, -1 and -2 will tend to contribute to the motion in opposite directions.

Poloidal coil. Consider now the diagram of Figure 2b, and suppose that this results from the projection of a poloidal coil in space. Since the central area has index $+1$ and the external lobes have all indices -1, by (5) we see that the resulting impetus component may amount to a negative value (depending on the relative contributions of the standard areas), giving rise to a possible backward motion in the negative direction of the normal to the plane of projection. Such strange type of motion has been actually found by numerical simulation by Barenghi *et al.* in 2006 [8], and confirmed in more recent work by Maggioni *et al.* [9, 10].

Trefoil knotting. A "thought experiment" to produce a trefoil vortex knot from the interaction and reconnection of vortex rings was conjectured by Ricca [11]. Upon collision (see Figure 3a), two vortex rings propagate one after the other to reconnect, thus forming a trefoil knot (Figure 3b). By assigning the indices $\mathcal{I}_j$ to the regions, it is possible to estimate the impulse associated with the different parts of the vortex in relation to their projected areas.

3.2. Multi-component systems: links

Rings. Two vortex rings of equal, but opposite, circulation move towards each other to collide (see left diagram of Figure 4). A finite number of reconnections take place in the colliding vortices, triggering the production of smaller vortex rings. Small rings are thus produced (right diagram of Figure 4). Actually this process has been realized by the head-on collision of coloured vortex rings in water by Lim & Nickels [12]. Since at the initial state linear momentum $\mathbf{P} = 0$ (for symmetry reason), we expect that this remains so till the very moment reconnections take place. The central diagram of Figure 4 represents (schematically) the graph in the plane of collision, at the reconnection time. By applying the index computation, we can estimate the signed areas contributions. By using (5) we see that the central region does not contribute to the momentum of the system, whereas the outer regions, contribute with opposite sign to the momentum of the emerging small vortex rings. The alternating signs of the outer regions indicate the production of smaller rings of opposite polarity, thus ensuring $\mathbf{P} = 0$ throughout the process. The generation and shoot-off of smaller rings from the plane of collision in opposite directions is in agreement with the experimental results of Lim and Nickels [12].

Hopf links. Finally, let us consider the projection of a Hopf link made by two vortex rings of circulation Γ_1 and

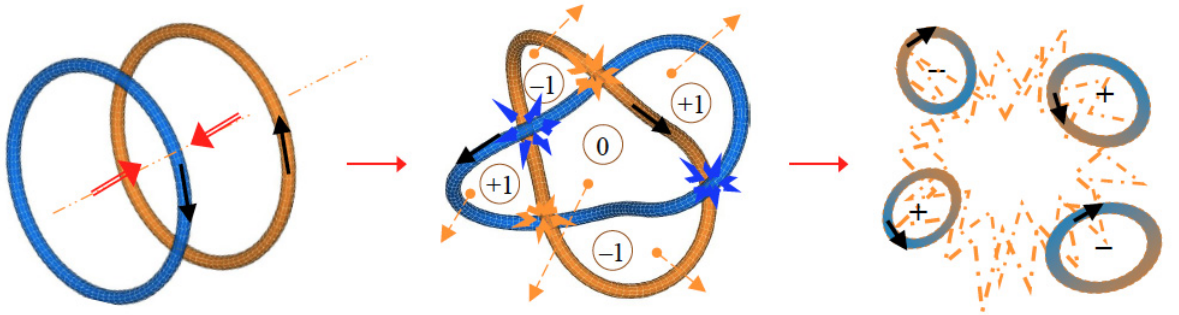

Fig. 4. (a) Two vortex rings interact and (b) reconnect to form a trefoil knot. The central region, having largest area and highest index, is likely to move more rapidly than the rest of the system in the normal direction of projection.

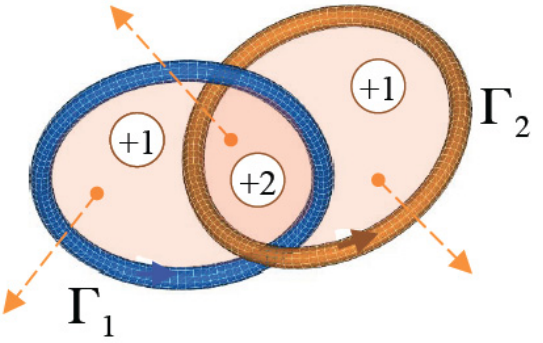

Fig. 5. Projection of a Hopf link formed by two vortex rings of circulation Γ_1 and Γ_2.

Γ_2 (see Figure 5). Since all the indices have same sign, all the graph regions contribute in the same direction to the impetus of the system. The central part, having the highest index, is likely to move faster than the rest of the system.

4. Momenta of a tangle of vortex filaments

From the examples considered in the previous section it is clear that the geometric interpretation of the momenta based on eqs. (6) and (7) can be extended to any complex graph resulting from the projection of a tangle $\mathcal{T} = \cup_i \mathcal{K}(\chi_i)$ of filaments in space. We can now state the geometric criterium for the computation of the momenta from geometric diagram information.

Theorem (Momenta in terms of signed area interpretation). *Let $\mathcal{T}$ be a vortex tangle under Euler equations. Then,*

the linear momentum $\mathbf{P} = \mathbf{P}(\mathcal{T}) = (P_x, P_y, P_z)$ *has components*

$$P_x = \Gamma \sum_{j=1}^{Z} \mathcal{I}_j A_{yz}(R_j) \,, \quad P_y = \dots \,, \quad P_z = \dots \,, \tag{10}$$

and the angular momentum $\mathbf{M} = \mathbf{M}(\mathcal{T}) = (M_x, M_y, M_z)$ *has components*

$$M_x = \frac{2}{3}\Gamma d_x \sum_{j=1}^{Z} \mathcal{I}_j A_{yz}(R_j) \,, \quad M_y = \dots \,, \quad M_z = \dots \,, \tag{11}$$

where $A_{yz}(R_j)$*,* $A_{zx}(R_j)$*,* $A_{xy}(R_j)$ *denote the standard areas of* R_j $(j = 1, \dots, Z)$*, for any projection plane normal to the component of the momenta of* $\mathcal{T}$*.*

Proof of the above Theorem is based on direct applications of (6), (7) and (9).

5. Conclusions

A method to compute linear and angular momenta of vortex filaments forming a complex network of curves in space has been presented. This method generalizes the original area interpretation of the momenta of vortex filaments omeomorphic to the standard circle put forward by Lord Kelvin in 1875, by a straightforward analysis on graphs resulting from standard diagram projections of the filaments in space. The method proposed here can be easily implemented in numerical codes and it has potential to become a useful complementary tool for real-time analysis of fundamental aspects of structural complexity,. These will include relationships between energy and morphology of vortex structures and energy transfers during re-structuring (after reconnections). Immediate applications in current work on vortex tangles [13] and vortex knots dynamics [9, 10] in superfluid helium are envisaged. This technique will complement further a set of measures based on algebraic, geometric and topological information that have been developed by Ricca and co-authors [14, 15, 16, 17] to investigate aspects of structural complexity in classical, quantum and magnetic systems.

Acknowledgements

I would like to thank Claude Weber for pointing out the Gauss-Olbers correspondence quoted in [7] and his comments on the signed area, and Keith Moffatt for his comments on an earlier version of this paper. I would also like to thank the Isaac Newton Institute for Mathematical Sciences for the kind hospitality and financial support provided through a Visiting Fellowship in Cambridge (UK).

References

[1] Kelvin, Lord (Thomson, W). Vortex statics. *Proc. Roy. Soc. Edin.* 1875 Session 1875–1876, 115–128.
[2] Arms RJ, Hama FR. Localized induction concept on a curved vortex and motion of an elliptic vortex ring, *Phys. Fluids* 1965 **8**, 553–559.
[3] Saffman PG. *Vortex Dynamics*. Cambridge University Press, Cambridge, 1991.
[4] Walmsley PM, Golov AI, Hall HE, Levchenko AA, Vinen WF. Dissipation of quantum turbulence in the zero temperature limit. *Phys. Rev. Lett.* 2007 **99**, 265302–265305.
[5] Golov AI, Walmsley PM. Homogeneous turbulence in superfluid 4He in the low-temperature limit: experimental progress. *J. Low Temp. Phys*. 2009 **156**, 51–70.
[6] Ricca RL. Momenta of a vortex tangle by structural complexity analysis. Physica D 2008 **237**, 2223–2227.
[7] Gauss CF. Letter to H. Olbers. Werke 1825 **8**, 398–400.
[8] Barenghi CF, Hänninen R, Tsubota M. Anomalous translational velocity of vortex ring with finite-amplitude Kelvin waves. *Phys Rev. E* 2006 **74**, 046303.

[9] Maggioni F, Alamri SZ, Barenghi CF, Ricca RL. Velocity, energy, and helicity of vortex knots and unknots. *Phys. Rev. E* 2010 **82**, 026309.
[10] Maggioni F, Alamri SZ, Barenghi CF, Ricca RL. Vortex knots dynamics in Euler fluids. In *Topological Fluid Dynamics II* (ed. K. Bajer *et al.*) IUTAM Procedia, this volume.
[11] Ricca RL. New developments in topological fluid mechanics. *Nuovo Cimento C* 2009 **32**, 185–192.
[12] Lim TT & Nickels TB. Instability and reconnection in head-on collision of two vortex rings, Nature **357** 1992, 225–227.
[13] Barenghi CF, Ricca RL, Samuels DC. How tangled is a tangle? *Physica D* 2001 **157**, 197–206.
[14] Ricca RL. New energy and helicity lower bounds for knotted and braided magnetic fields. *Geophys. Astrophys. Fluid Dyn.* 2012, on line: 10.1080/03091929.2012.681782.
[15] Liu X, Ricca RL. The Jones polynomial for fluid knots from helicity, *J. Phys. A: Math. & Theor.* 2012 **45**, 205501.
[16] Liu X & Ricca RL. Tackling fluid structures complexity by the Jones polynomial. In *Topological Fluid Dynamics II* (ed. K. Bajer *et al.*) IUTAM Procedia, this volume.
[17] Ricca RL. Structural complexity of vortex flows by diagram analysis and knot polynomials. In *Emergence, Complexity and Computation in Nature* (ed. I. Zelinka *et al.*), in preparation. Springer-ECC Series. Springer-Verlag, in press.